

Contents lists available at ScienceDirect

Journal of Energy Chemistry

journal homepage: www.elsevier.com/locate/jechem



http://www.journals.elsevier.com/

Syngas production by dry reforming of the mixture of glycerol and ethanol with CaCO₃

Chengxiong Dang^{a,b}, Shijie Wu^b, Guangxing Yang^b, Yonghai Cao^b, Hongjuan Wang^b, Feng Peng^a, Hao Yu^{b,*}

ARTICLE INFO

Article history: Received 30 April 2019 Revised 26 July 2019 Accepted 5 August 2019 Available online 7 August 2019

Keywords: Glycerol Ethanol CaCO₃ Dry reforming Syngas

ABSTRACT

The reduction of CO_2 emission is crucial for the mitigation of climate change. A considerable amount of industrial CO_2 can be absorbed in the form of carbonates through high-temperature sorption processes. In this regard, the efficient conversion of carbonates to value-added products will provide an economically viable method for the sustainable usage of carbon compounds. Herein, we report a promising solution involving the use of a glycerol and ethanol mixture as a hydrogen donor in the dry reforming process with $CaCO_3$ to produce syngas. A series of metal active components, including Ni, Fe, Co, Cu, Pt, Pd, Ru, and Rh, was used to promote this reaction. Ni showed comparable performance with that of Pd, but outperformed Co, Fe, Cu, Rh, Ru, and Pt. Approximately 100% conversion of glycerol and ethanol, $\sim 92\%$ selectivity of synthesis gas $(H_2$ and CO), and a H_2/CO ratio of ~ 1.2 were achieved over $CaCO_3$ containing 10 wt% Ni $(10Ni-CaCO_3)$. Meanwhile, the CO_2 concentration was less than 5 vol%, indicating that most of the CO_2 captured by the carbonate can be transformed into chemicals; however, they cannot simply be emitted. The CO_2 released from the decomposition of $CaCO_3$ not only adjusted the ratio of H_2 to CO but also eliminated cokes to guarantee the CO_2 absorption–conversion cyclic stability in the absence of steam and at high temperatures.

© 2019 Science Press and Dalian Institute of Chemical Physics, Chinese Academy of Sciences. Published by Elsevier B.V. and Science Press. All rights reserved.

1. Introduction

Constantly rising CO_2 levels in the atmosphere and the resultant concerns about the adverse effects on climate and environment warrant the development of strategies to prevent further CO_2 accumulation [1]. The application of CO_2 capture and storage (CCS) technology has been regarded as an efficient method for mitigating excessive CO_2 . CCS technology proposes that CO_2 could be captured from various point sources, including power plants and industrial facilities, subsequently concentrated and pressurized, and finally pumped underground into geological formations [2]. However, the commercialization of the technology remains challenging due to the high capital investment and ecological risk [3]. In this context, an alternative approach involves the conversion of the captured CO_2 to useful products, i.e., CO_2 capture and utilization (CCU) technology [3].

 CO_2 can potentially serve as an abundant C_1 resource to produce chemicals and fuels, such as CO [4–6], CH_3OH [7], CH_4 [8], and other low molecular-weight hydrocarbons [9]. In these developing processes, pure CO_2 is required for further conversion and utilization. However, most of the major emissions are composed of 5%–15% CO_2 and O_2 , N_2 , H_2O , etc. [10]. To extract pure CO_2 from the emissions, multiple steps, typically including capturing, desorption, storage, and conversion, are inevitable and energy-intensive; these steps complicate the operations and increase the costs [11].

In terms of CO_2 utilization, a simplified process integrating the CO_2 capture and conversion into a single step is highly desired [12]. Rao and co-workers reported that $CaCO_3$, as a CO_2 source, could be directly converted into CH_4 [13] and C1-C3 hydrocarbons [3] in hydrogen atmosphere, suggesting that the conversion of the CO_2 captured in carbonates was feasible. Farrauto and co-workers pointed out that the conversion of the CO_2 captured from a mixed CO_2 and N_2 gas could be achieved over $Ru-CaO-Al_2O_3$ dual-functional materials [1,14]. Hydrogen was introduced to convert carbonates in those works, which might be unconscionable

^a School of Chemistry and Chemical Engineering, Guangzhou University, Guangzhou 510006, Guangdong, China

^b School of Chemistry and Chemical Engineering, Guangdong Provincial Key Lab of Green Chemical Product Technology, South China University of Technology, Guangzhou 510640, Guangdong, China

^{*} Corresponding author. E-mail address: yuhao@scut.edu.cn (H. Yu).

and costly due to the current high price and low availability of hydrogen [3]. Müller and co-workers directly integrated CH₄ reforming with CO₂ capture to convert CO₂ and produce synthesis gas [15]. Steinfeld and co-workers conducted the dry reforming of methane using CaCO₃ to provide CO₂ in a single step [16]. Quite recently, we proposed an integrated process coupling the sorption-enhanced steam reforming of glycerol with CH₄ reforming of carbonates to co-produce high-purity hydrogen and syngas [12]. However, as a fossil fuel, CH₄ could not be a long-term solution for CO₂ utilization due to its limited supply and the unequal distribution of natural reserves [17].

One of the solutions involves the use of renewable sources as a hydrogen donor, particularly those from biomass. Crude glycerol has been considered as a very promising hydrogen donor [18], and it is the main by-product of the biodiesel manufacture process. It has been excessively supplied in recent years with the rapid growth of biodiesel production [19]. It is estimated that more than 7.66 million tons of crude glycerol will be produced in 2020. However, less than 2 million tons of crude glycerol is required to absorb the growing production [20]. Therefore, utilizing the biomass-derived glycerol as a hydrogen donor not only serves to reduce the costs of biodiesel, but also serves as an ideal outlet for the superfluous glycerol. Crude glycerol consists not only of glycerol but also of impurities, such as lower alcohols, soap, catalysts, salts, and other organics [21]. Although ethanol is not the main impurity, it exhibits properties similar to those of glycerol, which makes its separation difficult, particularly as a raw material for transesterification [22,23]. In addition, as an important means of upgrading crude glycerol, the bioconversion of crude glycerol to ethanol will produce glycerol-containing ethanol [24,25]. The utilization of a glycerol/ethanol mixture for the conversion of carbonates, with ethanol considered as a promising hydrogen donor, is quite interesting.

$$C_3H_8O_3 + CaCO_3 \rightarrow 4CO + CaO + 3H_2$$

$$C_2H_5OH + CaCO_3 \rightarrow 3CO + CaO + 3H_2$$

$$CaO + CO_2 \rightarrow CaCO_3$$

In this work, we used a glycerol/ethanol mixture as a hydrogen donor in the dry reforming process with $CaCO_3$ (CDR) to produce the syngas. Therefore, various active metals were introduced to fabricate dual-functional catalysts to enhance the dry reforming process. We demonstrated the possibility of direct conversion of CO_2 , which was fixed in the form of carbonates, with biomass-derived glycerol and ethanol, to produce syngas. The facile utilization of CO_2 provided a new path to the effective reduction of CO_2 emission with process integration and intensification.

2. Experimental

2.1. Synthesis of catalysts

We synthesized the catalysts by the incipient wetness impregnation method. In brief, 1 g of CaCO₃ was added into the aqueous solution, which contained desired metallic ions, and the solution was prepared by dissolving corresponding salts in 50 mL of deionized water at room temperature. After vigorous stirring for 60 min, all the samples were dried at 100 °C overnight and calcined in air at 500 °C for 2 h to obtain the xM-CaCO₃ catalysts, where x and M are the mass fraction of M and active metal, respectively.

2.2. characterizations

X-ray diffraction (XRD) patterns were recorded on a Rigaku D/max-IIIAX diffractometer with Cu $K\alpha$ radiation (40 kV and 40 mA)

TGA (STA449 NETZSCH) was used to investigate the amount of carbon deposited. To eliminate the effect of the $CaCO_3$ decomposition, the same sample was heated from room temperature (RT) to 900 °C at a rate of 10 °C/min, in N_2 and air atmosphere.

The amount of carbon deposited was calculated by the following:

Amount of carbon deposited (%) = $Mass_{loss, air} - Mass_{loss, N_2}$

where $\mathsf{Mass}_{\mathsf{loss},\mathsf{air}}$ and $\mathsf{Mass}_{\mathsf{loss},\mathsf{N}_2}$ correspond to the mass losses (TG) in the air and N2, respectively.

To study the carbon deposition of the catalyst, we conducted a CO_2 temperature-programmed reaction (CO_2 -TP) on the TP5080 apparatus equipped with a thermal conductivity detector (TCD). A portion (50 mg) of the catalysts was firstly treated in N_2 (30 mL/min) at 200 °C for 30 min. Subsequently, after cooling to ambient temperature, pure CO_2 (30 mL/min) was used for the CO_2 -TP reaction, followed by heating from RT to 900 °C at a rate of 10 °C/min.

The coking behavior on the surface of the catalyst during the reaction was characterized by field emission scanning electron microscopy (FESEM, Zeiss Merlin) at an acceleration voltage of 5 kV. Raman spectra were obtained using a LabRAM Aramis micro Raman spectrometer at an excitation wavelength of 632.8 nm, with a 2 μ m spot size.

2.3. Dry reforming reaction

The catalytic reactions were performed in a quartz tubular fixed bed reactor with I.D. of 10 mm and a length of 280 mm [12,26]. Typically, after heating the reactor to the desired temperature under N_2 atmosphere (30 mL/min), the aqueous glycerol/ethanol mixed solution was fed into the reactor at 0.02 mL/min using a high-pressure piston pump (Series II, LabAlliance), to initiate the catalytic reaction for 120 min. For the cyclic tests, $CaCO_3$ regeneration was carried out in the CO_2 (30 mL/min) atmosphere at 550 °C for 30 min, and the CDR reaction time was 70 min. The gaseous products were analyzed every 5 min using a gas chromatograph (with N_2 as the carrier gas) equipped with a TCD and a flame ionization detector (FID). A TDX-01 column was used for H_2 analysis in TCD. The FID coupled with a methanator was used to analyze the concentrations of CO_2 , CH_4 , C_2H_4 , and C_2H_6 .

The ratio of H_2 to CO $(R_{\rm H_2/CO})$ was calculated using the following formula:

$$R_{\rm H_2/CO} = \frac{[\rm H_2]}{[\rm CO]}$$

The summed selectivity of $\rm H_2$ and $\rm CO~(\it S_{\rm CO+H_2})$ was calculated using the following formula:

$$S_{CO+H_2}(\%) = \frac{[H_2] + [CO]}{[gaseous \, products]} \times 100$$

The syngas yield (Y_{CO+H_2}) was calculated using the following formula:

$$Y_{\text{CO+H}_2} = [F_{\text{CO}}]_{\text{out}} + [F_{\text{H}2}]_{\text{out}}$$

The CO_2 concentration (C_{CO_2}) in gaseous products was calculated using the following formula:

$$C_{CO_2}(\%) = \frac{[CO_2]}{[gaseous products] + [N_2]} \times 100$$

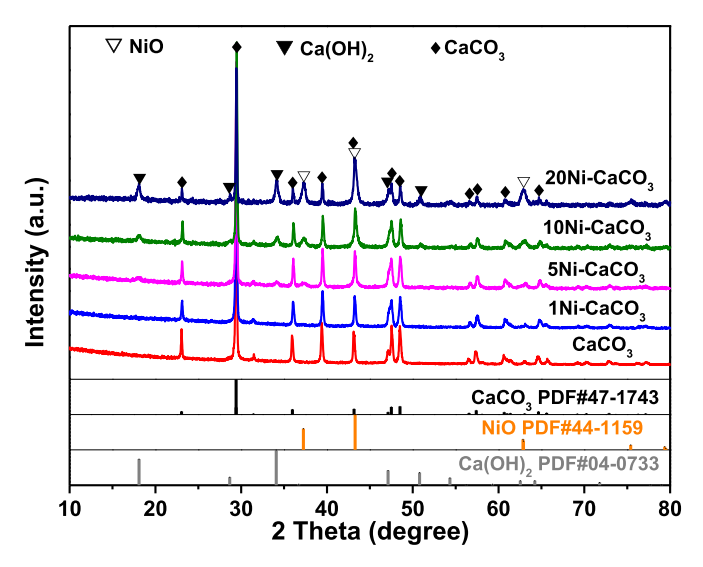


Fig. 1. XRD patterns of the calcined $Ni-CaCO_3$ catalyst with different Ni mass fractions.

The selectivities of carbon-containing species (CO, CO₂, CH₄, C_2H_4 , and C_2H_6) were calculated using the following formula:

$$S_i(\%) = \frac{[i]}{[gaseous \, products \, containing \, carbon]} \times 100$$

where [H₂], [CO], [CO₂], [N₂], [gaseous products], and [gaseous products containing carbon] represent the moles of H₂, CO, CO₂, N₂, gaseous products, and gaseous products containing carbon, respectively. [F_{CO}]_{out} and [F_{H_2}]_{out} represent the flows of CO and H₂ in the gaseous products.

Meanwhile, we averaged all sampling points to evaluate the performance throughout the reaction.

The conversions of glycerol and ethanol were analyzed using a high-performance liquid chromatograph (HPLC, Agilent 1260) equipped with a refractive index detector [27]. The conversions of glycerol ($X_{\rm gly}$) and ethanol ($X_{\rm eth}$) were calculated using the following formulas:

$$X_{\rm gly} = \frac{Glycerol_{\rm in} - Glycerol_{\rm out}}{Glycerol_{\rm in}} \times 100\%$$

$$X_{\text{eth}} = \frac{Ethanol_{\text{in}} - Ethanol_{\text{out}}}{Ethanol_{\text{in}}} \times 100\%$$

where $\mathit{Glycerol}_{in}$, $\mathit{Glycerol}_{out}$, $\mathit{Ethanol}_{in}$, and $\mathit{Ethanol}_{out}$ represent the moles of glycerol and ethanol fed in and out of the reaction system.

3. Results and discussion

3.1. Catalytic dry reforming of glycerol/ethanol

The composition of the CaCO₃-supported metal catalyst was determined by XRD. Taking Ni–CaCO₃ as an example, the characteristic peaks of NiO are clearly presented in Fig. 1, indicating that the Ni precursor had been transformed to NiO under the calcination conditions. Meanwhile, the existence of Ca(OH)₂ can be determined as being probably due to the hydroxylation reaction between CaO and the moisture in the air [28].

To understand the CDR performance of the glycerol/ethanol mixture, the typical evolutions of CO₂ concentration, H₂/CO ratio, and syngas yield were recorded. As shown in Fig. 2, the profiles could be divided into two characteristic stages. In the dry reforming stage, relatively low values of $R_{\rm H_2/CO}$ (\sim 1.2) were observed due

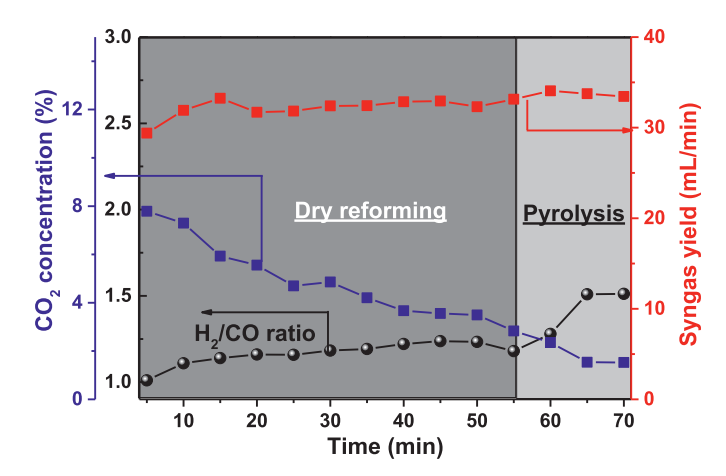


Fig. 2. CO_2 concentration, H_2/CO ratio, and syngas yield profiles of the $10Ni-CaCO_3$ catalyst during the first cycle of CDR. Reaction conditions: 1 g of the catalyst, E/G=4, 30 mL/min N_2 , 765 °C, 70 min.

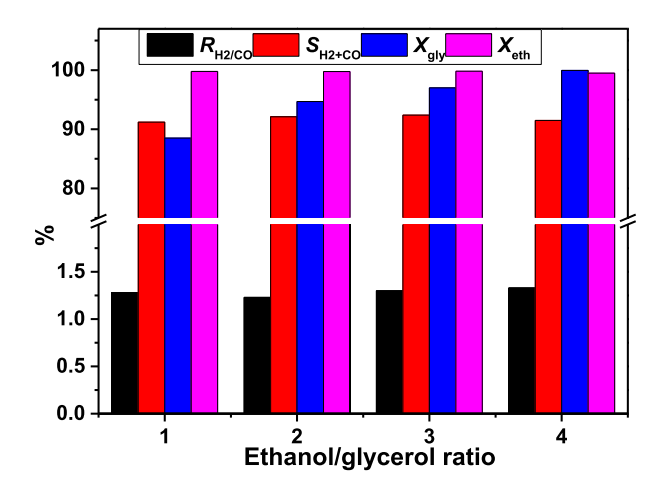


Fig. 3. Effect of the ethanol/glycerol molar ratio on the performance of CDR over the $10Ni-CaCO_3$ catalyst. Reaction conditions: 1 g of the catalyst, 30 mL/min N_2 , 750 °C; the data are averaged values during 120 min.

to the participation of the CO_2 released from the decomposition of $CaCO_3$ during the dry reformation of the glycerol/ethanol mixture. The decreasing CO_2 concentration indicated the variable rate of the CO_2 release at high temperatures. After the complete decomposition of $CaCO_3$, CO_2 no longer participated in the dry reforming. Subsequently, the process behaved similarly to the pyrolysis of the glycerol/ethanol mixture, and the negligible amount of CO_2 would be attributed to the pyrolysis process [29]. The $R_{\rm H_2/CO}$ difference between the dry reforming and pyrolysis stages evidenced the conversion of $CaCO_3$. Notably, during the decomposition of $CaCO_3$, the yield of syngas remained almost unchanged, and the CO_2 concentration was less than 8%, suggesting the direct involvement of carbonates in the production of syngas.

The effect of the molar ratio of ethanol to glycerol (E/G) on the performance of CDR is shown in Fig. 3. The E/G ratio slightly affects the average $\rm H_2/CO$ molar ratio for 120 min, which is \sim 1.3. Meanwhile, the selectivity of syngas ($\rm H_2$ and CO) was maintained at \sim 92% with changing the E/G ratio. At all the E/G ratios, the conversion of ethanol was nearly complete, while the conversion of glycerol was improved from 88.51% to 99.96% with the increment of the E/G ratio. The different conversions of glycerol and ethanol were attributed to the relatively high decomposition temperature of glycerol [26,30,31]. Nevertheless, the high conversions and

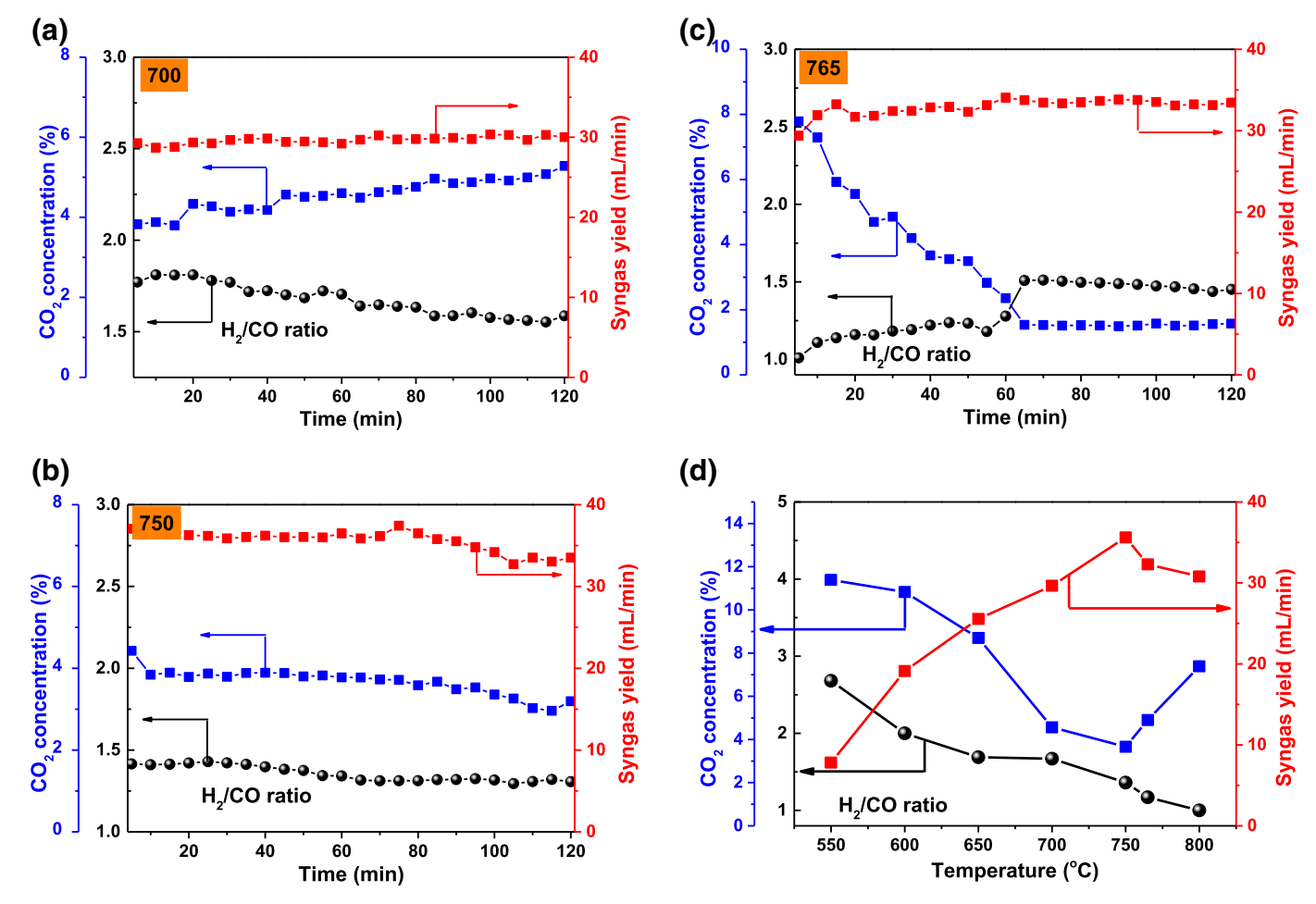


Fig. 4. (a–c) Time courses of CDR over the 10Ni-CaCO_3 catalyst. Reaction conditions: 1 g of the catalyst, 30 mL/min N_2 , E/G = 4, 120 min. (d) Effect of the temperature on the averaged performance of CDR over the 10Ni-CaCO_3 catalyst during the dry reforming stage. The evaluation times of the average results were 120, 55, and 35 min for temperatures lower than $765 \, ^{\circ}\text{C}$, $765 \, ^{\circ}\text{C}$, and $800 \, ^{\circ}\text{C}$, respectively.

stable syngas selectivity indicate that syngas could be reliably produced by this approach. Considering the increased viscosity of the feedstock containing a high fraction of glycerol, we fixed the E/G ratio at 4 for further study, to reduce the operational complexity of the reactor.

Fig. 4 presents the effect of temperature on the CDR of the glycerol/ethanol mixture. At low temperatures (<700 °C) (Fig. S1(a–c) and Fig. 4(a)), no two stages were distinctly observed during 120 min, since the decomposition of CaCO₃ was slow, and the main reaction was the catalytic cracking of glycerol/ethanol. In the cracking process, the dehydrogenation of glycerol and ethanol was preferred over that of Ni [32,33], leading to the relatively high $R_{\rm H_2/CO}$ (>1.5). Meanwhile, the conversions of glycerol and ethanol (Fig. S2) and the yield of syngas were low. Considerably high CO₂ concentrations were observed at relatively low temperatures, indicating the possibility of coking via the Boudouard reaction of CO, which may deactivate the catalysts. The coking also resulted in the gradual decrease in $R_{\rm H_2/CO}$.

As shown in Fig. 4(b,c), at temperatures higher than 750 °C, the transition from dry reforming to cracking can be clearly observed, corresponding to the dramatic increase in $R_{\rm H_2/CO}$ [34]. When the temperature was further elevated to 800 °C (Fig. S1(d)), a considerably high CO₂ concentration and large variation of $R_{\rm H_2/CO}$ were observed during the dry reforming stage. This result was attributed to the violent decomposition of CaCO₃ to release a large amount

of gaseous CO_2 at high temperatures, which deteriorated the utilization of carbonates. The involvement of $CaCO_3$ in the production of syngas can be verified by the XRD patterns of the catalyst after the reaction (Fig. S3). At temperatures lower than 750 °C, the used catalysts were composed of $CaCO_3$ and Ni, while only CaO was detected at temperatures higher than 750 °C, indicating that the consumption of carbon in $CaCO_3$ occurred above 750 °C through either simple decomposition or dry reforming. This result might be related to the favorable decomposition temperature of $CaCO_3$, which was often reported at \sim 760 °C or above [35,36].

Fig. 4(d) compares the average results of the syngas yield, CO_2 concentration, and $R_{H_2/CO}$ during the dry reforming stage at different temperatures. The highest syngas yield and the lowest CO_2 concentration were achieved at 750 °C. In addition, a steady production of syngas could be achieved within 120 min with almost unchanged yield and composition, implying the trade-off between the decomposition and conversion of $CaCO_3$. Similarly, steady production of syngas could be achieved at 765 °C, despite that the comparatively high temperature enhanced the decomposition of $CaCO_3$, which resulted in the continuous decrease in the CO_2 content during the dry reforming. Nevertheless, the comparatively high temperature allowed for the relatively high conversion of carbonates, leading to the low $R_{H_2/CO}$ of \sim 1.2, which is suitable for the production of dimethyl ether [37]. Considering the relatively fast conversion of carbonates and glycerol/ethanol at

Table 1. Effect of metals on the performance of CDR. Reaction conditions: 1 g of the catalyst, 30 mL/min N_2 , E/G=4, 765 °C, and 120 min. All the values are averaged for 120 min

		S _{H2+CO}	S _{CO2}	S _{CH4}	S _{C2H4}	S _{C2H6}	$C_{ m glycerol}$	$C_{ m ethanol}$
Catalysts	R _{H2/CO} (%)							
5Fe-CaCO ₃	1.18	64.58	13.53	29.99	8.71	1.87	97.45	97.15
5Ni-CaCO ₃	1.21	87.92	4.73	18.45	0.05	0.22	99.45	99.11
5Co-CaCO ₃	1.10	78.80	5.91	26.34	0.95	1.98	98.30	98.26
5Cu-CaCO₃	1.26	58.92	16.44	31.44	10.92	2.18	94.28	94.50
1Pd-CaCO ₃	1.12	83.4	4.38	25.20	-	-	90.54	90.41
1Pt-CaCO ₃	1.25	68.84	12.97	23.35	12.03	1.68	90.11	89.80
1Rh-CaCO ₃	1.26	65.11	15.10	25.69	12.15	1.61	88.59	84.85
1Ru-CaCO ₃	1.26	62.54	14.70	27.81	13.00	1.76	86.87	82.60

Table 2. Effect of the Ni dosage on the performance (average value) of CDR. Reaction conditions: 1 g of the catalyst, 30 mL/min N_2 , E/G=4, 765 °C, 120 min.

		S _{H2+CO}	S _{CO2}	S _{CH4}	S_{C2H4}	S_{C2H6}	$C_{ m glycerol}$	$C_{ m ethanol}$
Catalysts	R _{H2/CO}				(%)			
CaCO ₃ 1Ni-CaCO ₃ 5Ni-CaCO ₃ 10Ni-CaCO ₃ 20Ni-CaCO ₃	1.1 1.15 1.21 1.33 1.55	55.3 81.08 87.92 92.9 93.7	17.20 6.37 4.73 5.88 5.75	31.46 26.35 18.45 8.78 8.60	11.81 0.56 0.05 -	2.38 1.40 0.22 -	82.70 88.09 99.45 99.97 99.83	78.24 89.10 99.11 99.82 99.75

high temperatures (see Figs. 4, S1, and S3), 765 °C was determined as the optimum reaction temperature in this study.

The effect of the metal on the CDR of the glycerol/ethanol mixture has been studied. In the absence of a metal, the bare CaCO₃ afforded the lowest selectivity toward syngas and conversion of glycerol/ethanol. Among conventional base metals, as shown in Table 1, the highest summed selectivity (87.92) for H₂ and CO was achieved over the 5Ni-CaCO3 catalyst. Meanwhile, the conversion of glycerol and ethanol were ~100%. This was owing to the high activity of Ni, which facilitated the C-C bond rupture [38]. Although Ni is generally considered susceptible for coking, its selectivity toward C₂H₆ and C₂H₄, typical precursors of polymerized condensates [39], was the lowest, suggesting the resistance against coking. The performance of Co-CaCO₃ was close to that of Ni due to the similar catalytic reforming performances of Ni and Co [40], while Fe and Cu were inappropriate for the CDR reaction. For the noble metals, Pd slightly outperformed Ni in terms of conversion and syngas selectivity, while Pt, Ru, and Rh were less active than Ni was. Moreover, the performance could be improved with increasing the Ni dosage (Table 2), demonstrating the catalytic role of the transition metal on the CDR reaction.

3.2. Cyclic CDR-carbonation for CCU

In the context of CCU, the metal-supported carbonates need to be regenerated by the absorption of CO $_2$. It would be challenging to guarantee the structural stability of the catalyst after the CDR reaction. Five CDR-carbonation cycles were carried out to evaluate the stability of 10Ni-CaCO_3 under the optimized conditions. As displayed in Fig. 5, the $R_{\text{H}_2/\text{CO}}$ profile remains almost unchanged during the five cycles, while the syngas selectivity undergoes deterioration from $\sim 92\%$ to $\sim 85\%$, particularly at the beginning of the CDR reaction. Nevertheless, the conversion of glycerol/ethanol was nearly complete and the CO $_2$ selectivity was maintained lower than 6 vol% (Table S2). The slight deactivation was probably owing to the sintering of Ni particles and CaO [41]. Considering the absence of steam, these results are encouraging and show promise of CCU through this integrated technology.

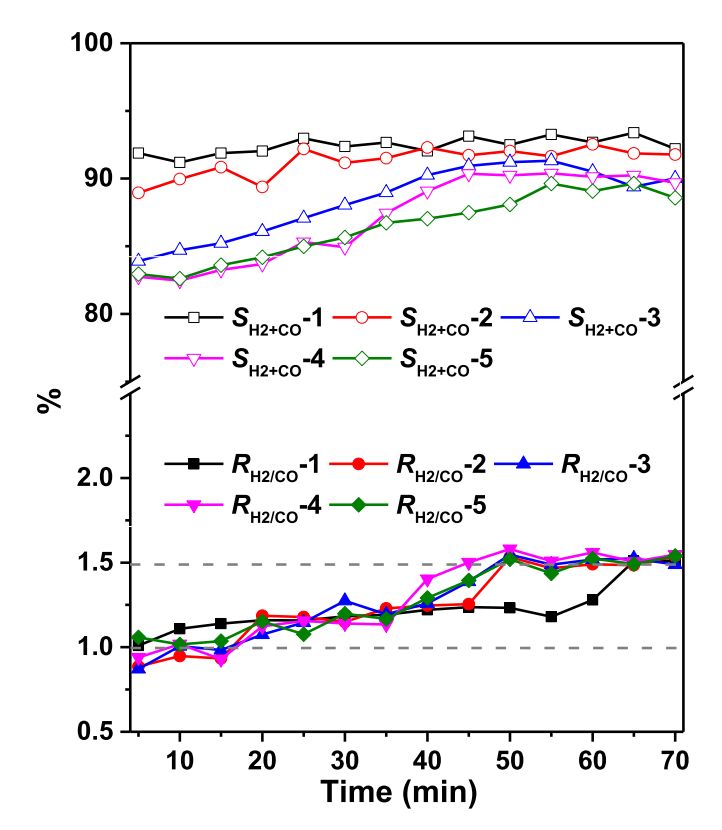


Fig. 5. $R_{\rm H_2/CO}$ and $S_{\rm H_2/CO}$ profiles during multiple CDR-carbonation cycles over 10Ni–CaCO₃. CDR reaction conditions: 1 g of the catalyst, E/G = 4, 30 mL/min N₂, 765 °C, 70 min. Carbonation conditions: 30 mL/min CO₂, 550 °C, 30 min.

Due to the importance of stability to the feasibility of this integrated technology, we focused intensively on understanding the deterioration of the CDR performance. Ni catalysts usually suffer from deactivation due to the formation of coke in the reforming reactions at high temperatures [42–45]. We conducted XRD studies to follow the deposition of carbon over the 10Ni–CaCO₃ catalyst at different reaction times. As shown in Figs. 6(a) and S4, the characteristic peaks of CaCO₃ decreased in intensity with the reaction time, while those from CaO increased in intensity. After 50 min, the conversion of CaCO₃ to CaO was nearly complete and the (002) peak at 26° from that indicative of graphite carbon could be observed simultaneously, evidencing the formation of coke. We ascribed this phenomenon to the elimination of coke in the presence of carbonates through the following reactions [26]:

$$CaCO_3 \rightarrow CaO + CO_2$$

$$CO_2 + C \rightarrow 2CO$$

The amount of carbon deposited was measured by TGA (Fig. 6(b)). After the reaction for 50 min, the carbon amount significantly increased from 0.45 wt% to 2.39 wt%, and further increased drastically to 19.31 wt% at 120 min. This result well supported the suppression of coking in the presence of CaCO₃. The fast formation of carbon deposits would rapidly deactivate the catalyst. The SEM results indicated that the carbon deposits were composed mainly of filamentous carbon or carbon nanotubes (Fig. 6(c)) [46].

The type of carbon species is another important factor that significantly affects the stability of the catalyst deactivation. The results of CO₂-TP showed the formation of different carbon species during the different periods of dry reforming. Four distinct regions in these curves can be identified (Fig. 7(a)). Zheng and co-workers

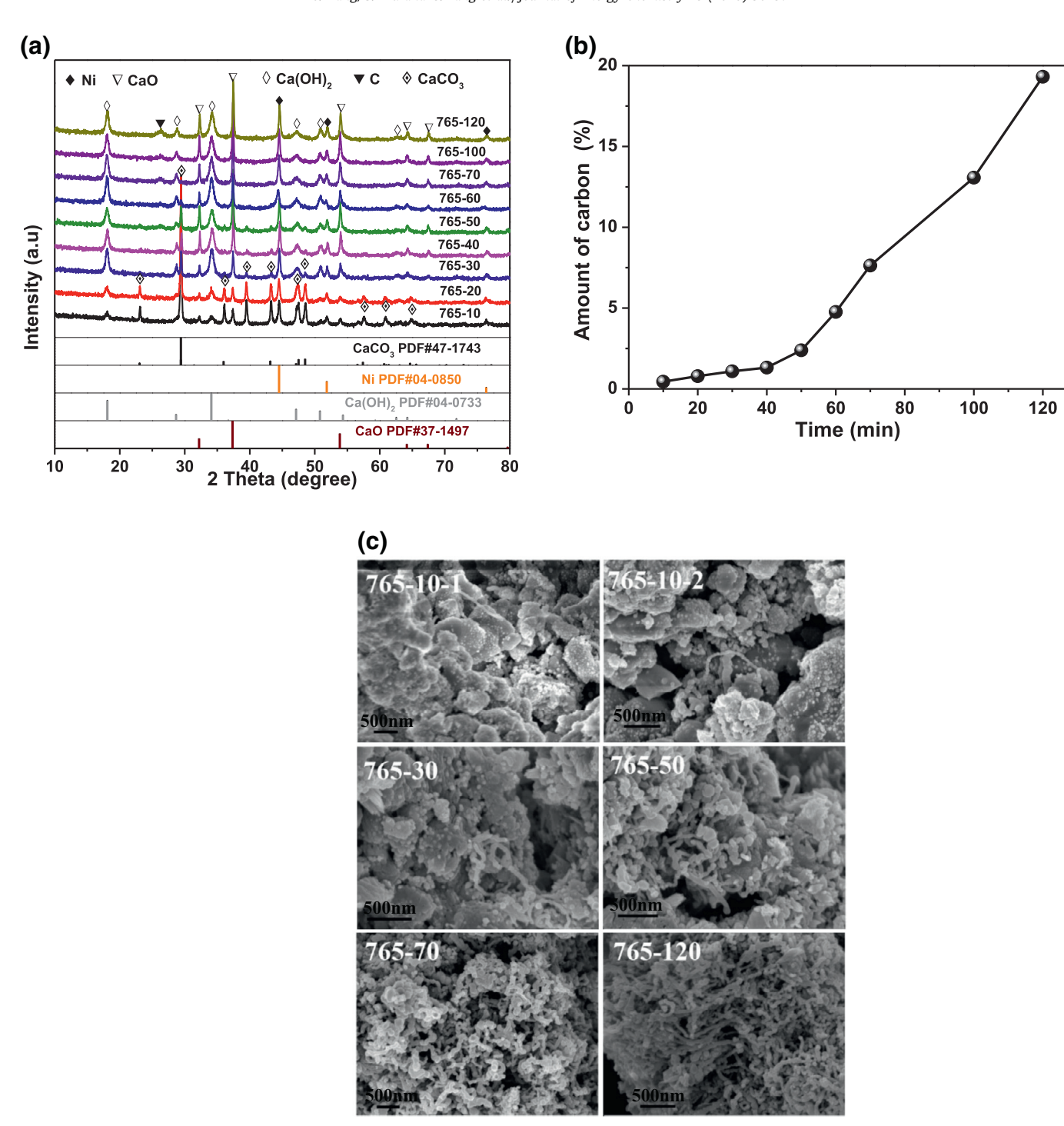
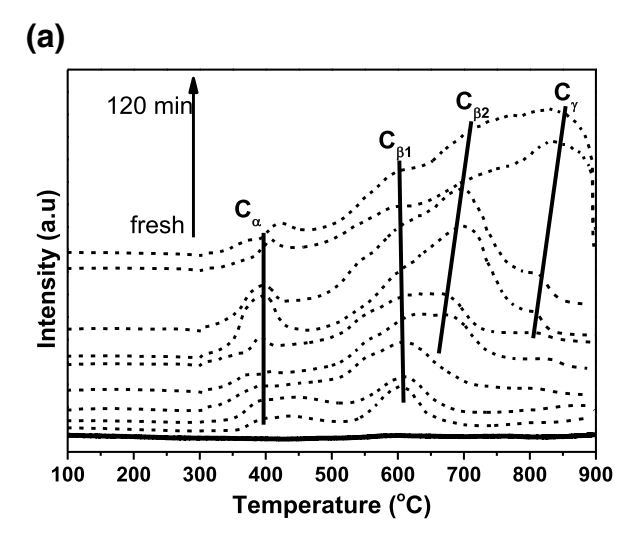


Fig. 6. (a) XRD patterns and (b) carbon content measured by the TGA of $10Ni-CaCO_3$ after the CDR reaction for 10, 20, 30, 40, 50, 60, 70, 100, and 120 min. (c) SEM images of $10Ni-CaCO_3$ after the CDR reaction for 10, 30, 50, 70, and 120 min. Reaction conditions: 1 g of the catalyst, E/G = 4, 30 mL/min N_2 , 765 °C.

[47] classified the carbon deposited as C_{α} , C_{β} , and C_{γ} , corresponding to the carbon with high, moderate and, low reactivities, respectively. The peak around 400 °C originates from the oxidation of C_{α} , which could be ascribed to the reactive intermediate of cokes that can be oxidized easily at low temperatures [48]. The C_{β} species is usually included in metal carbide, carbon nanotubes, graphene, and amorphous carbon [49]. In this work, the C_{β} species present a shoulder peak at temperatures from ~550 to 730 °C. The former $(C_{\beta 1})$ might be attributed to the transformation of the more active amorphous carbon [28], while the $C_{\beta 2}$ species could be recognized as originating from the graphite carbon with a relatively

high crystallinity. C_{γ} is the most inactive carbon species, which was stable until 800 °C, and which is highly relevant in the catalyst deactivation [47]. The Raman results (Fig. 7(b)) also confirmed the formation of carbon deposits with few defects at relatively long reaction times, as demonstrated by the comparatively low $I_{\rm D}/I_{\rm G}$ values.

These results indicate that the amount of coke species depends strongly on the reaction time. Prior to the depletion of CaCO₃, the carbon species consisted dominantly of C_{α} . After that, the amounts of $C_{\beta 1}$, $C_{\beta 2}$, and C_{γ} significantly increased and dominated the coke. This result confirms that the presence of CaCO₃ is



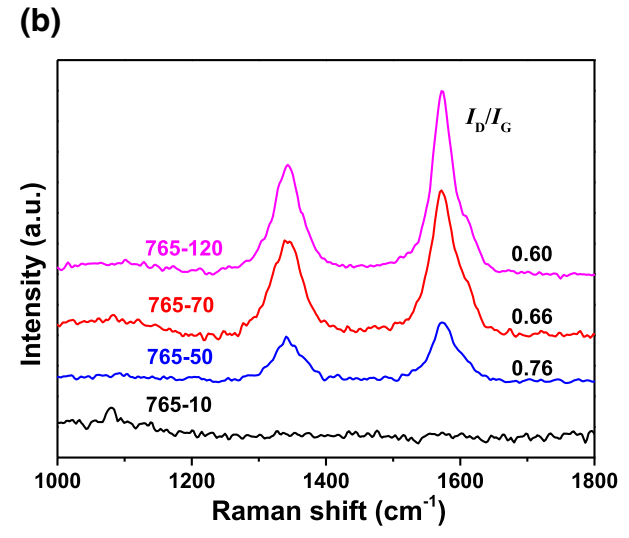


Fig. 7. (a) CO₂-TP profiles of fresh 10Ni-CaCO₃ and those after the CDR reaction for 10, 20, 30, 40, 50, 60, 70, 100, 110, and 120 min. (b) Raman spectra of 10Ni-CaCO₃ after the CDR reaction for 10, 50, 70, and 120 min. Reaction conditions: 1 g of the catalyst, E/G = 4, 30 mL/min N2, 765 °C.

beneficial for suppressing the coking process. More importantly, it reduces the formation of highly stable carbon species, which may block active sites. Due to the high reactivity of C_{α} with CO_2 , the next carbonation operation at 550 °C may effectively eliminate the coke to regenerate the Ni catalyst to guarantee the recyclability of the CDR-carbonation.

4. Conclusions

We have studied syngas production by the dry reforming of a glycerol/ethanol mixture, with CaCO₃ as a CO₂ carrier. The direct utilization of CaCO3 was found to be feasible in this process, and the CO2 released from the decomposition of CaCO3 could adjust the H₂/CO ratio. Among the active metals, including Ni, Co, Fe, Cu, Rh, Ru, Pt, and Pd, Ni was the most promising candidate on account of its excellent performance and low price. Under the optimum conditions, ~100% conversion of glycerol and ethanol, a summed H₂ and CO selectivity of \sim 92%, and a H₂/CO ratio of \sim 1.2 could be achieved over the 10Ni-CaCO₃ catalyst. Meanwhile, five dry reforming-regeneration cycles demonstrated the robustness of this integrated technology. The stability can be attributed to the elimination of coking by the release of CO₂ from CaCO₃. The results here provide a new path to utilizing CO₂ in the form of carbonates.

Acknowledgments

This work was supported by the Guangdong Natural Science Foundation (2017A030312005) and Science and Technology Program of Guangzhou City (201707010058).

Supplementary materials

Supplementary material associated with this article can be found, in the online version, at doi:10.1016/j.jechem.2019.08.002.

Reference

- [1] M.S. Duyar, S. Wang, M.A. Arellano-Treviño, R.J. Farrauto, J. CO₂ Util. 15 (2016)
- [2] A. Goeppert, M. Czaun, J.P. Jones, G.K. Surya Prakash, G.A. Olah, Chem. Soc. Rev. 43 (2014) 7995-8048.
- [3] D. Jagadeesan, Y. Sundarayya, G. Madras, C.N.R. Rao, RSC Adv. 3 (2013) 7224.
- [4] F.V. Vazquez, P. Pfeifer, J. Lehtonen, P. Piermartini, P. Simell, V. Alopaeus, Ind. Eng. Chem. Res. 56 (2017) 13263-13273.
- [5] C. Panaritis, M. Edake, M. Couillard, R. Einakchi, E.A. Baranova, J. CO2 Util. 26 (2018) 350-358.
- [6] B.H. Qin, Y.H. Li, H.Q. Fu, H.J. Wang, S.Z. Chen, Z.L. Liu, F. Peng, ACS Appl. Mater. Inter. 10 (2018) 20530-20539.
- [7] Q.H. Low, N.W.X. Loo, F. Calle-Vallejo, B.S. Yeo, Angew. Chem. Int. Edit. 58 (2018) 2256-2260.
- [8] X. Guo, Z. Peng, M. Hu, C. Zuo, A. Traitangwong, V. Meeyoo, C. Li, S. Zhang, Ind. Eng. Chem. Res. 57 (2018) 9102–9111.
- J.Y. Wang, A.F. Zhang, X. Jiang, C.S. Song, X.W. Guo, J. CO₂ Util. 27 (2018) 81–88.
- [10] H.A. Patel, J. Byun, C.T. Yavuz, ChemSusChem 10 (2017) 1303–1317.
- [11] M.A. Naeem, A. Armutlulu, Q. Imtiaz, F. Donat, R. Schäublin, A. Kierzkowska, C.R. Müller, Nat. Commun. 9 (2018) 1-11.
- [12] C. Dang, S. Wu, Y. Cao, H. Wang, F. Peng, H. Yu, Chem. Eng. J. 360 (2019) 47–53.
 [13] D. Jagadeesan, M. Eswaramoorthy, C.N.R. Rao, ChemSusChem 2 (2009) 878-882.
- [14] M.S. Duyar, M.A.A. Treviño, R.J. Farrauto, Appl. Catal. B-Environ. 168-169 (2015) 370-376.
- [15] S.M. Kim, P.M. Abdala, M. Broda, D. Hosseini, C. Copéret, C. Müller, ACS Catal. 8 (2018) 2815-2823.
- [16] V. Nikulshina, M. Halmann, A. Steinfeld, Energy Fuel 23 (2009) 6207-6212.
- [17] A.W. Westbrook, D. Miscevic, S. Kilpatrick, M.R. Bruder, M. Moo-Young, C.P. Chou, Biotechnol. Adv. 37 (2019) 538–568.
- [18] J. Remón, P. Arcelus-Arrillaga, L. García, J. Arauzo, Appl. Energy 228 (2018) 2275-2287
- [19] C.A. Schwengber, H.J. Alves, R.A. Schaffner, F.A. da Silva, R. Sequinel, V.R. Bach, R.J. Ferracin, Renew. Sustain. Energy Rev. 58 (2016) 259-266.
- [20] M.R. Monteiro, C.L. Kugelmeier, R.S. Pinheiro, M.O. Batalha, A. da Silva César, Renew. Sustain. Energy Rev. 88 (2018) 109-122.
- [21] N.L. Reddy, K.K. Cheralathan, V.D. Kumari, B. Neppolian, S.M. Venkatakrishnan, ACS Sustain. Chem. Eng. 6 (2018) 3754-3764.
- [22] P. Verma, G. Dwivedi, M.P. Sharma, Fuel 188 (2017) 586-594.
- [23] J.J. Torres, N.E. Rodriguez, J.T. Arana, N.A. Ochoa, J. Marchese, C. Pagliero, J. Cleaner Prod. 141 (2017) 641-647.
- [24] X. Liu, P.R. Jensen, M. Workman, Bioresour. Technol. 104 (2012) 579-586.
- [25] C. Varrone, B. Giussani, G. Izzo, G. Massini, A. Marone, A. Signorini, A. Wang, Int. J Hydrog. Energy 37 (21) (2012) 16479-16488.
- [26] C. Dang, H. Yu, H. Wang, F. Peng, Y. Yang, Chem. Eng. J. 286 (2016) 329–338.
 [27] X. Ning, Y. Li, H. Yu, F. Peng, H. Wang, Y. Yang, J. Catal 335 (2016) 95–104.
- [28] C. Dang, H. Wang, H. Yu, F. Peng, Appl. Catal. A 533 (2017) 9-16.
- [29] F. Viteri, A. López, Á. Millera, R. Bilbao, M.U. Alzueta, Fuel 236 (2019) 820-828.
- A. Lima da Silva, I.L. Müller, Int. J. Hydrog. Energy 36 (2011) 2057-2075. [31] E.B. Pereira, P.R. de la Piscina, N. Homs, Bioresour. Technol. 102 (2011) 3419-3423.
- [32] Y.C. Sharma, A. Kumar, R. Prasad, S.N. Upadhyay, Renew. Sustain. Energy Rev. 74 (2017) 89-103.
- [33] M.N.N. Shahirah, B.V. Ayodele, J. Gimbun, S.S. Lam, C.K. Cheng, Appl. Therm. Eng. 112 (2017) 871-880.
- [34] A. López Ortiz, R.B. Pallares Sámano, M.J. Meléndez Zaragoza, V. Collins-Martínez, Int. J. Hydrog. Energy 40 (2015) 17172-17179.
- [35] M. Sánchez-Cantú, M. de Lourdes Ruiz Peralta, A.B. Galindo-Rodríguez, E. Puente-López, E. Rubio-Rosas, C.M. Gómez, F. Tzompantzi, Fuel 198 (2017)
- [36] N. Chiwaye, L.L. Jewell, D.G. Billing, D. Naidoo, M. Ncube, N.J. Coville, Mater. Res. Bull. 56 (2014) 98-106.
- W. Schakel, G. Oreggioni, B. Singh, A. Strømman, A. Ramírez, J. CO₂ Util. 16 (2016) 138-149.
- [38] M. Ni, D.Y.C. Leung, M.K.H. Leung, Int. J. Hydrog. Energy 32 (2007) 3238–3247. X. Huang, C. Dang, H. Yu, H. Wang, F. Peng, ACS Catal. 5 (2015) 1155-1163.
- M. Konsolakis, Z. Ioakimidis, T. Kraia, G. Marnellos, Catalysts 6 (2016) 39.
- P. Xu, Z. Zhou, C. Zhao, Z. Cheng, Catal. Today 259 (2016) 347-353.
- A.A. Goncalves, P.B. Faustino, J.M. Assaf, M. Jaroniec, ACS Appl. Mater. Inter. 9 (2017) 6079-6092.

- [43] V. Palma, C. Ruocco, E. Meloni, A. Ricca, Int. J. Hydrog. Energy 42 (2017) 1598-1608.
- [44] D.F.P. Suffredini, V.V. Thyssen, P.M.M. de Almeida, R.S. Gomes, M.C. Borges, A.M. Duarte de Farias, E.M. Assaf, M.A. Fraga, S.T. Brandão, Catal. Today 289 (2017) 96-104.
- [45] S. Koc, A.K. Avci, Fuel Process. Technol. 156 (2017) 357–365.
- [46] N.D. Charisiou, K.N. Papageridis, G. Siakavelas, V. Sebastian, S.J. Hinder, M.A. Baker, K. Polychronopoulou, M.A. Goula, Catal. Today 319 (2019) 206–219.
 [47] J. Guo, H. Lou, X. Zheng, Carbon (NY) 45 (2007) 1314–1321.
 [48] Z.L. Zhang, X.E. Verykios, Catal. Today 21 (1994) 589–595.
 [49] R. Zhou, X. Cao, X. Jia, J. Wang, C.-j. Liu, Chem. Eng. Sci. 194 (2019) 22–28.